Draft version July 20, 2016
Preprint typeset using LaTeX style emulateapj v. 12/16/11

DARK ENERGY AND MODIFIED GRAVITY

Zhongxu Zhai, Michael Blanton
Center for Cosmology and Particle Physics, Department of Physics, New York University, 4 Washington Place, New York, NY 10003, USA

Draft version July 20, 2016

ABSTRACT

Subject headings: large scale structure of universe, dark energy

1. INTRODUCTION

Since it was first discovered more than one decade ago (Riess et al. 1998; Perlmutter et al. 1999), the accelerated expansion of the universe has been one of the greatest mysteries in modern physics. The attempt to explain this phenomena has motivated us to propose various theoretical models. Among these plentiful candidates, the cosmological constant is the mathematically simplest solution which is interpreted as a new energy component in the universe. Although the cosmological constant is able to fit the observation with high confidence, it has a key problem that its value indicated from cosmology is different from the prediction of quantum field theory by an order of ~ 120 (see review by Weinberg 1989).

The alternative approaches to solve the cosmic acceleration rather than cosmological constant involves the introduction of the exotic energy matter component in the universe, the so called dark energy. The possible models include the dynamical vacuum energy, cosmic fluid, scalar field and so on. Rather than introducing new energy matter content, the other route is to change the geometrical structure of spacetime, i.e modified gravity theories. These string motivated or General Relativity motivated models introduce the large scale correction and modification of late time evolution of the universe, such as $f(R)$ gravity, $f(T)$ gravity, extra dimension, Galileon cosmology etc. We describe and explore several classes of these models in this paper, but refer to recent reviews: Peebles & Ratra 2003; Copeland et al. 2006; Linder 2008; Silvestri & Trodden 2009; Caldwell & Kamionkowski 2009; Weinberg et al. 2013; Joyce et al. 2015 and references therein.

2. COSMOLOGICAL MODELS AND DATA SETS

A homogeneous and isotropic universe is described by the Friedman-Robertson-Walker metric

$$ds^2 = -dt^2 + a^2(t)\left[\frac{dr^2}{1-kr^2} + r^2 d\Omega^2\right], \tag{1}$$

where $a(t)$ is the scale factor related to redshift z as $a(t) = (1+z)^{-1}$ and k is the curvature parameter. In General Relativity (GR), the evolution of the universe is governed by the field equation which connects the Einstein tensor and energy momentum tensor

$$G_{\mu\nu} = 8\pi G T_{\mu\nu}, \tag{2}$$

where G is the Newton gravitational constant. This equation gives the expansion of the universe as

$$\frac{H^2}{H_0^2} = E^2(z) = \frac{\rho(a)}{\rho_0} + \Omega_k a^{-2}, \tag{3}$$

where $H \equiv \dot{a}/a$ is the Hubble parameter, $E(z)$ is a dimensionless function which is sometimes called expansion factor, $\rho(a)$ is the total energy density, the subscript '0' denotes the value at present ($z = 0$). The density parameter of a given energy density is defined as

$$\Omega_x = \frac{\rho_x}{\rho_{\rm crit}} = \frac{8\pi G}{3H^2}\rho_x. \tag{4}$$

The normalization of the Hubble parameter gives the relation between the density parameter and curvature parameter

$$\sum_x \Omega_x + \Omega_k = 1, \tag{5}$$

where the summation is over all the energy and matter components in the universe. Throughout this paper, the density parameters refer to the current values at $z = 0$ unless otherwise denoted.

In the standard ΛCDM model, the dark energy is a constant in space and time, therefore we can write the Hubble parameter as

$$\frac{H^2}{H_0^2} = E^2(z) = \Omega_m(1+z)^3 + \Omega_r(1+z)^4 + \Omega_\Lambda + \Omega_k(1+z)^2, \tag{6}$$

where Ω_m includes the contribution from cold dark matter (CDM) and baryons, Ω_r represents radiation and relativistic matter, and Ω_Λ is the cosmological constant. For simplicity and the efficiency of the calculation, we assume the neutrinos are massless and contribute the same as radiation.

In the next section, we briefly introduce the dark energy and modified gravity models that are explored in this paper.

2.1. *Cosmological models*

2.1.1. *Parameterization of equation of state w*

The equation of state w of a perfect fluid is defined as the ratio of its pressure and density

$$w = p/\rho. \tag{7}$$

For cosmological constant, we have $w = -1$. Therefore the simplest generalization is $w = const.$ (Turner & White 1997; Chiba et al. 1997) which changes the third term on the right hand side of Eq.(6) to be

$$\Omega_\Lambda(1+z)^{3(1+w)}. \tag{8}$$

In this kind of cosmology (hereafter XCDM), the DE models with a conical kinetic term have $-1 < w < -1/3$, while models with $w < -1$ are phantom dark energy (Faraoni & Dolgov 2002; Caldwell 2002; Caldwell et al. 2003). Thus $w = -1$ is a critical value to differentiate the phantom property of the dark energy.

The generalization of constant w is to assume it is a function of time. The first model considered in this paper is the CPL parameterization (Chevallier & Polarski 2001; Linder 2003), which is the first order Taylor expansion of the scale factor at the present epoch

$$w = w_0 + w_1(1-a) = w_0 + w_1\frac{z}{1+z}, \tag{9}$$

where w_0 and w_1 are two parameters. The corresponding term for dark energy Eq. (8) needs to be

$$\Omega_\Lambda \exp\Big(3\int_0^z \frac{1+w}{1+z'}dz'\Big). \tag{10}$$

Another type of parameterization is proposed in Jassal et al. (2005) (hereafter JBP):

$$w = w_0 + w_1\frac{z}{(1+z)^2}. \tag{11}$$

Note that this model has quite different asymptotic behavior in high redshift compared with CPL parameterization.

The last model considered here is a simple linear function of redshift z (Cooray & Huterer 1999; Weller & Albrecht 2002; Astier 2001)

$$w = w_0 + w_1 z, \tag{12}$$

which may not converge in high redshift. These three parameterizations have the same parameter space and similar behavior in the late time universe. Note that the integral in Eq. (10) can be calculated analytically, therefore no numerical routine is needed which is important in the following computation.

2.1.2. *Casimir effect*

This kind of cosmology involves a negative radiation-like term in the expression of Hubble parameter Eq. (6)

$$-\Omega_c(1+z)^4, \tag{13}$$

where $\Omega_c > 0$ is a constant (Godłowski & Szydłowski 2006). In principle, there are different interpretations of this term. The first is the Casimir effect which comes from the consequence of quantum fluctuation (Bordag et al. 2001). The second is called 'dark radiation' introduced by the extra dimension in the universe. For instance, in the Randall and Sundrum scenario (Randall & Sundrum 1999), the restriction of the field equation on the brane induces this term. The third interpretation is the global rotation which is from the Newtonian analogue of the Firedmann equation (Senovilla et al. 1998; Godłowski & Szydłowski 2006)

2.1.3. *Cardassian expansion*

Cardassian expansion model is first proposed by Freese & Lewis (2002), which is a modification of the Friedmann equation from $H^2 = A\rho$ to

$$H^2 = A\rho + B\rho^n, \tag{14}$$

with parameter $n < 2/3$. This equation can be written in terms of the density parameters as (assuming the curvature and radiation are ignored)

$$\frac{H^2}{H_0^2} = \Omega_m(1+z)^3 + (1-\Omega_m)(1+z)^{-3n}. \tag{15}$$

So it is equivalent to the XCDM model with $w = n - 1$. This model is generalized in Wang et al. (2003) by introducing one more free parameter $q > 0$. The resulting Hubble parameter is expressed as

$$\frac{H^2}{H_0^2} = \Omega_m(1+z)^3\Big(1 + \frac{\Omega_m^{-q}-1}{(1+z)^{3q(1-n)}}\Big)^{\frac{1}{q}}. \tag{16}$$

This model is also called 'Modified Polytropic Cardassian' (MP Cardassian) when it is treated as a fluid. However, this model can also arise from the self-interaction of dark matter, or embedding the observable brane into a higher dimensional universe (Davis et al. 2007).

2.1.4. *Pseudo-Nambu Goldstone Boson*

This model is motivated by the potential $V(\phi \propto [1 + \cos(\phi/F)])$ of the scalar field (Frieman et al. 1995; Dutta & Sorbo 2007). The dark energy in this model is parameterized by its equation of state (Basilakos et al. 2010)

$$w = -1 + (1+w_0)(1+z)^{-F}, \tag{17}$$

where w_0 and F are free parameters. When $w_0 = -1$, this model becomes standard ΛCDM model. Because $z > 0$, the second term also vanishes as F becomes large, so we restrict the range of F to be within [0,8] as adopted in literature.

2.1.5. *QCD ghost dark energy*

The QCD ghost dark energy is proposed in Urban & Zhitnitsky (2010a, 2009a,b, 2010b); Ohta (2011). The key ingredient of this model is the Veneziano ghost field which is required to exist for the resolution of the U(1) problem in QCD (Witten 1979; Veneziano 1979; Rosenzweig et al. 1980; Kawarabayashi & Ohta 1980; Kawarabayashi & Ohta 1981; Ohta 1981). The ghost fields make no contribution in the flat Minkowski space, but they give rise to a vacuum energy density once they are in a curved space or time-dependent background. Consider a flat FRW universe, the energy density of DE in this model is given by $\rho_{\rm DE} = \alpha H + \beta H^2$, where α and β are constants (Cai et al. 2012). After the redefinition of the parameters, we can write the Friedmann equation of the QCD ghost dark energy model as

$$\frac{H(z)}{H_0} = \kappa + \sqrt{\kappa^2 + \frac{\Omega_m(1+z)^3 + \Omega_r(1+z)^4}{\gamma}}, \tag{18}$$

where $\kappa = (1 - (\Omega_m + \Omega_r)/\gamma)/2$. Therefore this model has one more free parameter γ compared with ΛCDM model.

2.1.6. *Early dark energy*

In many of the models, dark energy is important only in late time universe. However, it is possible for some models that the dark energy can track the evolution of the dominant component in the universe. Therefore the dark energy is able to produce imprint during the early

time of the universe. We consider a generic parameterization of such early dark energy models as proposed by Doran & Robbers (2006). In this model, the density parameter of dark energy is given as a function of $a = (1+z)^{-1}$

$$\Omega_{\rm de} = \frac{\Omega^0_{\rm de} - \Omega^{\rm e}_{\rm de}(1-a^{-3w_0})}{\Omega^0_{\rm de} + \Omega_m a^{3w_0}} + \Omega^{\rm e}_{\rm de}(1-a^{-3w_0}), \quad (19)$$

where $\Omega^{\rm e}_{\rm de}$ and $\Omega^0_{\rm de}$ are the dark energy density parameter at early times and at present respectively. Therefore this model is fully characterized by these two parameters and w_0 which is the effective value of the equation of state. The Hubble parameter is given by

$$\frac{H^2(a)}{H_0^2} = \frac{\Omega_m a^{-3} + \Omega_r a^{-4}}{1-\Omega_{\rm de}}. \quad (20)$$

Note that this model approaches ΛCDM model when $w_0 = -1$ and $\Omega^{\rm e}_{\rm de}$ goes to zero.

2.1.7. *Slow roll dark energy*

The late time acceleration of the universe is similar in some sense to inflation during the early time. Therefore it is possible that these two phenomena come from the same physical mechanism. Based on this idea, Gott & Slepian (2011); Slepian et al. (2014) propose a simple dark energy model which can also be used to detect the deviation of w from -1. This model class is a slowly rolling scalar field with potential $\frac{1}{2}m^2\phi^2$, and the dark energy is parameterized by the equation of state

$$w(z) = -1 + \delta w(z) \approx \delta w_0 \times H_0^2/H^2(z), \quad (21)$$

and therefore

$$\frac{H^2(z)}{H_0^2} = \Omega_m(1+z)^3 + \Omega_{\rm de}\Big[\frac{(1+z)^3}{\Omega_m(1+z)+\Omega_{\rm de}}\Big]^{\delta w_0/\Omega_{\rm de}}, \quad (22)$$

where δw_0 is the free parameter and the first-order of the deviation. This simple model can be easily falsified by the observational data and the difference from ΛCDM model can be detected.

2.1.8. *Polynomial CDM*

The energy density of dark energy can be described by a quadratic polynomial form with non-zero space curvature as an extended dark energy model. This model is highly flexible to represent the evolution of dark energy at low redshift (Aubourg et al. (2015)). The Hubble parameter is given as

$$\frac{H^2(z)}{H_0^2} = \Omega_m(1+z)^3 + \Omega_k(1+z)^2 + \Omega_1(1+z)^2 + \Omega_2(1+z)^1 + (1-\Omega_m-\Omega_k-\Omega_1-\Omega_2), \quad (23)$$

where Ω_1 and Ω_2 are two extra parameters.

2.1.9. *Oscillation and Logarithm Hubble parameter*

Indeed, the Polynomial CDM model can also be treated as a parameterization of the Hubble parameter. For comparison, we also consider another two different models. The first class is the Oscillating Ansatz (OA) proposed by Nesseris & Perivolaropoulos (2004)

$$\frac{H^2(z)}{H_0^2} = \Omega_m(1+z)^3 + \Omega_k(1+z)^2 + a_1\cos(a_2z^2+a_3) + (1-\Omega_m-\Omega_k-a_1\cos a_3), \quad (24)$$

The three parameters a_1, a_2 and a_3 make this model highly flexible to fit the observational data. It is also believed that the oscillating expansion rate can help resolve the coincidence problem (Dodelson et al. 2000; Nesseris & Perivolaropoulos 2004).

The second model is the logarithm model, which is first proposed from $f(R)$ gravity constrained by cosmography (Capozziello et al. 2014). We leave the discussion of particular $f(R)$ gravity in Sec. 2.1.16 and treat this model as a simple parameterization of the Hubble parameter

$$\frac{H^2(z)}{H_0^2} = \Omega_m(1+z)^3 + \Omega_k(1+z)^2 + \log(\alpha+\beta z), \quad (25)$$

where α and β are parameters with $\alpha = \exp(1-\Omega_m-\Omega_k)$, so only β is the free parameter.

2.1.10. *Chaplygin gas*

Chaplygin gas (CG) was first introduced in aerodynamics in 1904. It is applied to cosmology by Kamenshchik et al. (2001) as an unified fluid of dark matter and dark energy which has equation of state

$$p = -\frac{A}{\rho}, \quad (26)$$

where p and ρ are respectively pressure and energy density in a comoving reference frame, and A is a positive constant. The Chaplygin gas model is found to have an amusing connection with string theory and it can be obtained from Nambu-Goto action in the light-cone parameterization (Bordemann & Hoppe 1993).

Subsequently, this model is extended to be the Generalized Chaplygin gas (GCG) which has the equation of state (Bento et al. 2002; Bilić et al. 2002)

$$p = -\frac{A}{\rho^\alpha}, \quad (27)$$

where α is a new parameter with $0 < \alpha < 1$. In this model, the pressure in high redshift is negligible, while at late times both the pressure and energy density are constant. Therefore this single fluid can describe the matter-dominated universe until late time acceleration. This model can also arise from a complex scalar field whose action can be written as a generalized Born-Infeld action corresponding to a "perturbed" d-brane in a $(d+1,1)$ spacetime (Bento et al. 2002).

GCG model is also extended by adding a barotropic term, referred as Modified Chaplygin gas model (Benaoum 2002, hereafter MCG), with the equation of state

$$p = B\rho - \frac{A}{\rho^\alpha}, \quad (28)$$

where B is the a new constant. As mentioned above, these classes of Chaplygin gas model were first proposed as a unified description of dark matter and dark energy. However, the study of perturbation theory implies that this kind of model has odd behavior with current

cosmological data (Bean & Doré 2004; Giannantonio & Melchiorri 2006). Therefore, it is reasonable to assume that the Chaplygin gas only contributes to the dark energy component. After redefinition of the parameter $A_s = \frac{A}{1+B}\frac{1}{\rho_0^{1+\alpha}}$, where ρ_0 is the current energy density of dark energy, the Hubble parameter for MCG model can be written as

$$\frac{H^2(z)}{H_0^2} = \Omega_m(1+z)^3 + \Omega_k(1+z)^2 + (1-\Omega_m-\Omega_k) \quad (29)$$
$$[A_s + (1-A_s)(1+z)^{3(1+B)(1+\alpha)}]^{\frac{1}{1+\alpha}}.$$

The GCG model corresponds to $B = 0$, and the CG model corresponds to $B = 0$ and $\alpha = 1$.

2.1.11. *Interacting DE and DM*

In typical cosmological models, including all of those discussed above, the dark matter and dark energy are assumed to evolve independently. However, some scalar field models can couple to the ordinary matter or dark matter (Amendola 2000; Farrar & Peebles 2004). This kind of interaction of the dark sector can help resolve the coincidence problem. The researches on this model can be widely found in literatures: Zimdahl et al. (2001); Dalal et al. (2001); Tocchini-Valentini & Amendola (2002); Chimento et al. (2003); Caldera-Cabral et al. (2009); Bean et al. (2008) and references therein. In general, the interaction between the dark sector can be tracked by the observation. On the other hand, some interaction model can mimic the expansion of the ΛCDM model which is not distinguishable from the distance measurements, such as supernovae, baryon acoustic oscillation etc. In this case, we need to take into account observations from the growth of perturbation, since in general, the coupled dark energy model can not mimic the expansion and growth at the same time (Huterer et al. 2015). In this paper, we consider such models proposed in Fay (2016). The interaction between the dark sector is described by

$$\bar{H}^2 \propto \bar{\rho}_m + \bar{\rho}_{\rm de} \quad (30)$$
$$\bar{\rho}'_m + 3\bar{\rho}_m = \bar{Q}/\bar{H} \quad (31)$$
$$\bar{\rho}'_{\rm de} + 3(1+\bar{w})\bar{\rho}_{\rm de} = -\bar{Q}/\bar{H}, \quad (32)$$

where the bar denotes the interacting quantity, $\bar{Q}$ characterizes the interaction term, and the prime means the derivative with respect to $\ln a$. The particular models are specified by the equation of state of interaction dark energy $\bar{w}$ which together with $\rho_{\rm de}$ and $\bar{H}$ determines $\bar{Q}$. We consider two models in this paper as detailed in Fay (2016)

$$\text{Model I}: \quad \bar{w} = constant \quad (33)$$
$$\text{Model II}: \quad \bar{w} = \bar{w}_0 + \bar{w}_1 \ln a, \quad (34)$$
$$(35)$$

where $\bar{w}_0$ and $\bar{w}_1$ in Model II are constants.

2.1.12. *Weakly-coupled canonical scalar field*

As inflation, the late time acceleration of the universe can be explained by a scalar field once a potential function is explicitly written. Huang et al. (2011) introduces a three-parameter approximation of the equation of state $w(z;\epsilon_s,\epsilon_\infty,\zeta_s)$ which allows trajectories from a wide class of scalar field potentials

$$w = -1+\frac{2}{3}\Big[\sqrt{\epsilon_\infty}+(\sqrt{\epsilon_s}-\sqrt{2\epsilon_\infty})\big[F\big(\frac{a}{a_{\rm eq}}\big)+\zeta_s F_2\big(\frac{a}{a_{\rm eq}}\big)\big]\Big]^2, \quad (36)$$

where ϵ_s is the "slope parameter" defined as $\epsilon_s \equiv \epsilon_V|_{a=a_{\rm eq}}$ which measures the slope of the potential. ϵ_∞ is the "tracking parameter" which is defined from $\epsilon_\infty \equiv \epsilon_V\Omega_{\rm de}|_{a\to 0}$. The third parameter ζ_s captures the time-dependence of ϵ_V as a higher order correction, which is poorly constrained by the current and forecasted data. Therefore we set it to be zero in the following discussion. The function $F(x)$ is defined as

$$F(x) = \frac{\sqrt{1+x^3}}{x^{3/2}} - \frac{\ln(x^{3/2}+\sqrt{1+x^3})}{x^3}. \quad (37)$$

$a_{\rm eq}$ is the scale factor of "matter-DE" equality which can be approximated by a fitting formula (Huang et al. 2011). In our paper, we discuss the one-parameter ($\epsilon_\infty = 0$) and two-parameter classes respectively.

2.1.13. *Holographic dark energy*

The holographic principle plays an important role in modern theoretical physics. In quantum gravity, the entropy of a system scales with its surface area instead of volume (see 't Hooft 1993; Susskind 1995; 't Hooft 2001; Bekenstein 1973, 1981, 1994; Hawking 1976 and references therein), which contradicts the prediction from effective field theory where the entropy is an extensive quantity. The reconciliation is suggested in Cohen et al. (1999) by introducing a relationship between the UV and IR cut-off and thus an energy bound. However, this approach fails to produce the current cosmic acceleration as pointed out in Hsu (2004). The solution of this problem is suggested in Li (2004) which is to use the future event horizon as the characteristic length scale. The resulting holographic dark energy model (HDE) has energy density

$$\rho_{\rm de} = 3c^2 M_{\rm PL}^2 L^{-2}, \quad (38)$$

where c is a numerical constant, $M_{\rm PL} = 1/\sqrt{8\pi G}$ is the reduced Planck mass and L is related to the characteristic length scale. The Friedmann equation can be written as

$$\frac{H^2(z)}{H_0^2} = \frac{\Omega_m(1+z)^3}{1-\Omega_{\rm de}}, \quad (39)$$

where $\Omega_{\rm de}$ is determined through (Huang & Li 2004; Zhang & Wu 2007)

$$\frac{d\Omega_{\rm de}}{dz} = -\Omega_{\rm de}\frac{1-\Omega_{\rm de}}{1+z}\Big(1+\frac{2}{c}\sqrt{\Omega_{\rm de}}\Big) \quad (40)$$

Similar to HDE, Cai (2007) proposes the agegraphic dark energy model (ADE) motivated by the Karolyhazy relation (Karolyhazy 1966; Maziashvili 2007b,a). The dark energy density is determined by a time scale T

$$\rho_{\rm de} = 3n^2 M_{\rm PL}^2 T^{-2}, \quad (41)$$

where n is a constant to parameterize uncertainties. The original ADE model applies the age of the universe as the time scale. However, it is found that this model has difficulty to dominate the universe as pointed out in Wei

& Cai (2008). Therefore we consider the new agegraphic dark energy which uses the "conformal time" instead of the age of the universe. The solution is also expressed as a differential equation

$$\frac{d\Omega_{\rm de}}{dz} = -\Omega_{\rm de}\frac{1-\Omega_{\rm de}}{1+z}\Big(3-\frac{2(1+z)}{n}\sqrt{\Omega_{\rm de}}\Big). \quad (42)$$

Rather than using the length scale or time scale as the IR cut-off, Gao et al. (2009) propose another possibility: the length scale is given by the average radius of Ricci scalar curvature, $R^{1/2}$ (hereafter RDE). Different from the HDE and ADE models, the Hubble parameter of this model can be expressed analytically which is convenient in numerical solutions

$$\frac{H^2(z)}{H_0^2} = \frac{2\Omega_m}{2-\alpha}(1+z)^3+\Omega_k(1+z)^2+\Big(1-\Omega_k-\frac{2\Omega_m}{2-\alpha}\Big)(1+z)^{4-\frac{2}{\alpha}}, \quad (43)$$

where α is a constant to be determined.

2.1.14. *Quintessence scalar field model*

Scalar field can naturally arise in particle physics including string theory. It is also a direct generalization of cosmological constant which can play the role of dark energy. A quintessence field is such a scalar field with standard kinetic energy and minimally coupled to gravity. In a spatially flat FRW universe, the evolution of a scalar field ϕ is governed by the Friedmann equation Eq. (3) and Klein-Gorden equation

$$\ddot{\phi} + 3H\dot{a} + \frac{dV}{d\phi}, \quad (44)$$

where the dot denotes derivative with respect to cosmic time t. This model is completed by specifying the potential. In order to have acceleration, the potential needs to be flat. In this paper, we consider two types of potential

$$\begin{aligned} &\text{Model I}: V \propto \phi^{-n} \\ &\text{Model II}: V \propto \exp(-\lambda\phi), \end{aligned} \quad (45)$$

where the proportionality can be determined by the initial conditions, n and λ are the parameters. Model I is originally proposed by Ratra & Peebles (1988); Peebles & Ratra (1988); Caldwell et al. (1998). The solution from this model can alleviate the fine-tuning problem (Watson & Scherrer 2003). Model II is first motivated by the anomaly of the dilatation symmetry in the particle physics (Wetterich 1988). This potential can give rise to the accelerated expansion, as well as the scaling solution (Copeland et al. 1998; Barreiro et al. 2000) in which the energy density of dark energy is proportional to the matter.

2.1.15. *DGP cosmology*

As a modified gravity theory, DGP model is proposed by Dvali et al. (2000) as a braneworld model where our universe is a 4-dimensional brane embedded in a 5-dimensional bulk. It differs from the RS braneworld model (Randall & Sundrum 1999; Randall & Sundrum 1999) by a curvature term on the brane. We consider this model as detailed in Lombriser et al. (2009), the Hubble parameter can be written as

$$\frac{H^2(z)}{H_0^2} = \Big(\sqrt{\Omega_m(1+z)^3+\Omega_r(1+z)^4+\Omega_\Lambda+\Omega_{r_c}}+\sigma\sqrt{\Omega_{r_c}}\Big)^2 + \Omega_k(1+z)^2, \quad (46)$$

where the density parameters have the same meaning as ΛCDM model. $\sigma = +1$ refers to the self-accelerating branch (sDGP) which has late time acceleration without a cosmological constant. $\sigma = -1$ is the normal branch (nDGP) where the DGP modifications slow the expansion rate, therefore a cosmological constant is required to achieve late-time acceleration. Here

$$\sqrt{\Omega_{r_c}} = \frac{1}{2H_0 r_c} = \sigma\frac{\Omega_{\rm DGP}}{2\sqrt{1-\Omega_k}}, \quad (47)$$

where $\Omega_{\rm DGP} = 1-\Omega_m-\Omega_r-\Omega_k-\Omega_\Lambda$, and r_c is the crossover distance which governs the transition from 5D to 4D scalar-tensor gravity.

2.1.16. *f(R) gravity*

$f(R)$ gravity is a non-trivial modification of GR which replaces the Ricci scalar in the Einstein-Hilbert action by a non-linear function. A detailed introduction of this theory is given in Sotiriou & Faraoni (2010) and references therein. This model has the action

$$S = \int d^4x\sqrt{-g}\Big[\frac{R+f(R)}{2\mu^2}+\mathcal{L}_{\rm m}\Big], \quad (48)$$

where R is the Ricci scalar, $\mu^2 \equiv 8\pi G$ and $\mathcal{L}_{\rm m}$ is the Lagrangian of matter. This model is completed once the functional form of $f(R)$ is specified. However, a viable model should succeed a series tests, including the stability of the matter perturbation, the stability of a late-time de-Sitter point, the solar system test and so on. A lot of attentions have paid in this direction, some particular models and valuable results, including theoretical and observational investigations are obtained (Capozziello & Fang 2002; Nojiri & Odintsov 2003; Capozziello et al. 2003; Cognola et al. 2005; Amendola et al. 2007b,a; Hu & Sawicki 2007; Starobinsky 2007; Li & Barrow 2007; Zhao et al. 2011). In this paper, we consider the designer model introduced by Song et al. (2007); Lombriser et al. (2012) instead of restricting to particular classes of $f(R)$ gravity. This model mimics the expansion history of the ΛCDM model due to the fact that the function of $f(R)$ has sufficient flexibility. Therefore this model can be distinguished by the dynamics of the linear perturbation. The solution of this model is parameterized in terms of the Compton wavelength parameter

$$B = \frac{f_{RR}}{1+f_R}R'\frac{H'}{H}, \quad (49)$$

evaluated at $B_0 \equiv B(\ln a = 0)$, where $f_R \equiv df/dR$, $f_{RR} \equiv d^2f/dR^2$, and the prime denotes the derivative with respect to $\ln a$.This parameter indicates the modification of gravity, and $B_0 = 0$ recovers the standard gravity. The condition of stability requires $B_0 \geq 0$ (Song et al. 2007; Sawicki & Hu 2007; Lombriser et al. 2012).

2.1.17. *f(T) gravity*

$f(T)$ gravity is based on the old formulation of the teleparallel equivalent of general relativity (Einstein

1928; Unzicker & Case 2005; Hayashi & Shirafuji 1979; Arcos & Pereira 2004; Maluf 1994). The key ingredient in this formulation is the torsion tensor which plays the role as Ricci tensor in general relativity. The natural extension of this formulation is to generalize the Lagrangian to be a function of T which is the equivalent quantity of R in general relativity and $f(R)$ gravity (Ferraro & Fiorini 2007, 2008; Bengochea & Ferraro 2009; Linder 2010). Different from $f(R)$ gravity, the field equation in $f(T)$ theory is second-order rather than fourth-order which may have pathological behaviors. In general, the corresponding action of $f(T)$ gravity is

$$S = \frac{1}{16\pi G}\int d^4xe[T + f(T)], \tag{50}$$

where $e = \det(\mathrm{e}^{\mathrm{A}}_{\mu}) = \sqrt{-\mathrm{g}}$, and e^A_μ is the vierbein fields. Note that this theory gives ΛCDM model when $f(T) =$ constant.

Consider a flat FRW universe, the resulting Friedmann equation can be written as (Nesseris et al. 2013)

$$E^2(z) = \Omega_m(1+z)^3+\Omega_r(1+z)^4+(1-\Omega_m-\Omega_r)y(z), \tag{51}$$

where $y(z)$ is a function of redshift z dependent on the particular $f(T)$ model. In this paper, we consider the following specific $f(T)$ models appeared in literatures.

Model I: the power-law model (Bengochea & Ferraro 2009)

$$f(T) = \alpha(-T)^b, \tag{52}$$

where α and b are parameters. The function in the Friedmann equation is

$$y(z) = E^{2b}(z). \tag{53}$$

Model II: the exponential model as $f(R)$ gravity (Nesseris et al. 2013; Linder 2009)

$$f(T) = \alpha T_0(1 - e^{-T/(bT_0)}), \tag{54}$$

with α and b are parameters and

$$y(z) = \frac{1-(1+\frac{2E^2}{b})e^{-E^2/b}}{1-(1+\frac{2}{b})e^{-1/b}}. \tag{55}$$

Model III: the exponential model proposed by Linder (2009)

$$f(T) = \alpha T_0(1 - e^{-\sqrt{T/T_0}/b}), \tag{56}$$

where α and b are parameters, and

$$y(z) = \frac{1-(1+\frac{E}{b})e^{-E/b}}{1-(1+\frac{1}{b})e^{-1/b}}. \tag{57}$$

Bamba et al. (2011) propose a logarithmic model

$$f(T) = \alpha T_0\sqrt{(\frac{T}{qT_0})}\ln(\frac{qT_0}{T}), \tag{58}$$

where α and q are model parameters. The Hubble parameter in this model is independent from the α or q, and it coincides with the flat sDGP model without cosmological constant. Therefore the analysis of sDGP model is equivalent to this model. However, this model has different dynamical behavior which is represented by the perturbation equation (Nesseris et al. 2013).

Model IV: the hyperbolic-tangent model proposed by Wu & Yu (2011)

$$f(T) = \alpha(-T)^n\tanh\frac{T_0}{T}, \tag{59}$$

where α and n are model parameters. We also obtain

$$y(z) = E^{2(n-1)}\frac{2\mathrm{sech}^2(\frac{1}{E^2})+(1-2n)E^2\tanh(\frac{1}{E^2})}{2\mathrm{sech}^2(1)+(1-2n)\tanh(1)}. \tag{60}$$

This model is different from the previous 3 models that it can't restore to ΛCDM for any value of the parameters.

2.1.18. *Galileon cosmology: Tracker solution*

Galileon theory is a scalar field model introduced in Nicolis et al. (2009); Deffayet et al. (2009a,b). This model is inspired by the DGP model and its ability to produce the current acceleration without dark energy. This model is invariant under the Galileon symmetry in the Minkowski space-time, and keeps the field equation to be second order. The Galileon model considered in this paper is detailed in Nesseris et al. (2010); de Felice et al. (2011). For numerical purpose, we consider the tracker solution which has the Hubble parameter

$$E^2(z) = \frac{1}{2}\Omega_k(1+z)^2+\frac{1}{2}\Omega_m(1+z)^3+\frac{1}{2}\Omega_r(1+z)^4 +\sqrt{\Omega_g+\frac{(1+z)^4}{4}\left[\Omega_m(1+z)+\Omega_k+\Omega_r(1+z)^2\right]^2}, \tag{61}$$

where $\Omega_g = 1-\Omega_m-\Omega_k-\Omega_r$. Note that this model has the same parameters as ΛCDM model.

2.1.19. *Kinetic gravity braiding model*

The kinetic braiding model is inspired from Galileon model (Deffayet et al. 2010), which introduces the extended self-interaction term $G(\phi, X)\Box\phi$ minimally coupled to gravity, where $G(\phi, X)$ is a function of ϕ and X with $X = -g^{\mu\nu}\nabla_\mu\phi\nabla_\nu\phi/2$. This model is further generalized in Kimura & Yamamoto (2011) as $G(\phi, X) \propto X^n$ and the original model corresponds to $n = 1$. In a flat FRW universe, the Friedmann equation is

$$E^2(z) = (1-\Omega_m-\Omega_r)E^{-\frac{2}{2n-1}}+\Omega_m(1+z)^3+\Omega_r(1+z)^4. \tag{62}$$

For $n = 1$, this model is the same as the track solution in Galileon model Eq. (61). For n is an arbitrary parameter, it is equivalent to the power-law $f(T)$ theory Eq. (53). This is an interesting property in the sense that these two models have different physical mechanisms. It means the measurements from the expansion history are not able to differentiate these theories, thus the study of the dynamical aspect is necessary.

2.2. *Data sets*

We now discuss the data sets we use in this paper. The explorations of the models are realized by different data combinations, which give important information of the tensions between the observables.

2.2.1. *BAO data*

The BAO data arise from the measurements of the correlation function based on different tracers. As an absolute distance measurements, the determination of the

BAO scale is based on an fiducial cosmology, which translates the the angular and redshift separations to comoving distances. In an anisotropic analysis, the measurement of the BAO scale constrains the comoving angular diameter distance $D_M(z)$ and the Hubble parameter $H(z)$ through

$$D_M(z)/r_d = \alpha_\perp D_{M,\rm fid}/r_{d,\rm fid}, \tag{63}$$

and

$$D_H(z)/r_d = \alpha_\parallel D_{H,\rm fid}/r_{d,\rm fid}, \tag{64}$$

where $D_H(z) = c/H(z)$, r_d is the sound horizon at the drag epoch z_d when photons and baryons decouple

$$r_d = \int_{z_d}^{\infty} \frac{c_s(z)}{H(z)} dz, \tag{65}$$

with the sound speed in the photon-baryon fluid $c_s(z) = 3^{-1/2}c[1+\frac{3}{4}\rho_b(z)/\rho_\gamma(z)]^{-1/2}$. The subscript "fid" refers to the quantity in the assumed fiducial model, $\alpha_\perp$ and $\alpha_\parallel$ are the ratios of the distances perpendicular and parallel to the line of sight.

An isotropic BAO analysis provides the measurement of an effective distance which is a combination of $D_{M(z)}$ and $D_H(z)$ (Eisenstein et al. 2005)

$$D_V = [zD_H(z)D_M^2(z)]^{1/3} \tag{66}$$

through

$$D_V(z)/r_d = \alpha D_{V,\rm fid}(z)/r_{d,\rm fid}, \tag{67}$$

where α is the ratio of the BAO scale to that predicted by the fiducial model.

The measurements of BAO come from the correlation of galaxies and Lyman α Forest (LyaF). In our calculation, the data adopted are taken from 6dFGS (Beutler et al. 2011), SDSS main galaxy sample (MGS, Ross et al. 2015), BOSS galaxies (Anderson et al. 2014), BOSS LyaF auto-correlation (Delubac et al. 2015), and BOSS LyaF cross-correlation (Font-Ribera et al. 2014). The likelihood calculations of these data are the same as *Aubourget al.* (2015) (as summarized in their Table II), and we refer the readers to this paper for more details.

2.2.2. *Linear growth data*

The growth of structure measurement is an important probe to test dark energy and modified gravity models, especially when the geometrical measurements are not able to distinguish them from ΛCDM model. For scales well within the Hubble radius, the growth of structure is governed by the equation

$$\ddot{\delta} + 2H\dot{\delta} - 4\pi G\rho_m\delta = 0, \tag{68}$$

where the dots are derivatives with respect to time, and $\delta \equiv \delta\rho_m/\rho_m$ is the matter density contrast. Note that this equation should be modified accordingly in the modified gravity theories, or when the interaction between dark energy and dark matter is taken into account. Examples can be found in Fay (2016); Tsujikawa (2007). The measurement of the growth is often represented by $f\sigma_8(z)$ where $f \equiv d\ln D/d\ln a$, with $D(z) \equiv \delta(z)/\delta(0)$, and $\sigma_8(z) = \sigma_8 D(z)$ is the power spectrum amplitude. The current value of σ_8 is a parameter to be fit. The solution of the above equation is obtained by setting the initial conditions at $z \approx 30$ when the universe is dominated by matter and thus we have $\delta \sim a$ [[references]]

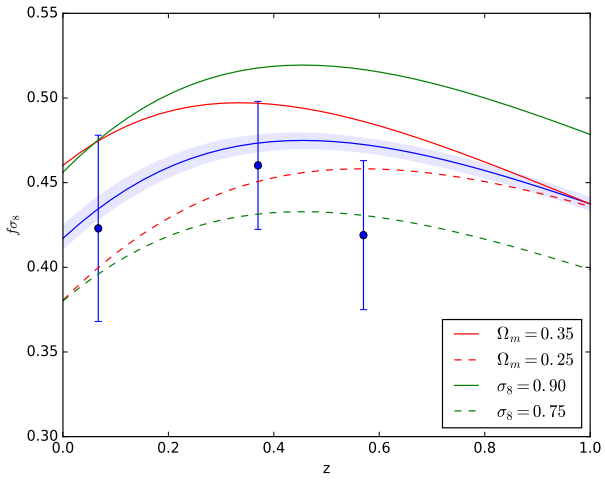

FIG. 1.— The linear growth data $f\sigma_8$ as a function of z. The solid blue line corresponds to the best-fit flat ΛCDM model from all the datasets, while the shaded region is the 1σ error. Green and red lines represent the effect of the parameter Ω_m and σ_8 respectively (other parameters are kept fixed at the best-fit values).

2.2.3. *Cosmic Microwave Background data*

The Cosmic Microwave Background measurements contain various important information and physics about the universe. Here we focus on the expansion history and linear perturbation of the universe, therefore the full CMB power spectrum is not computed in each model. Therefore we adopt the same strategy as Aubourg et al. (2015) to compress the CMB measurements to variables related to the expansion and linear growth. The geometrical aspect of this CMB compression is represented by the distance scale $D_M(1090)/r_d$ which is a BAO measurement at $z = 1090$, $\Omega_m h^2$ and $\Omega_b h^2$, the matter and baryon fractions of the universe, which determine the absolute length of the BAO ruler. The dynamical aspect is related to the variable $\sigma_8(z = 30)$ which is the amplitude of the matter power spectrum at the initial epoch of the perturbation Eq.(68). Therefore we find that the data vector of the CMB is

$$\mathbf{v} = \begin{pmatrix} \Omega_b h^2 \\ \Omega_m h^2 \\ D_M(1090)/r_d \\ \sigma_8(30) \end{pmatrix}. \tag{69}$$

In this paper, we use the publicly available `base_Alens` chains with the `planck_lowl_lowLike` dataset from the Planck dataset with low-l WMAP polarization (Planck Collaboration et al. 2014) [1]. Note that in the computation of $\sigma_8(30)$ from the Planck chains, we apply the late time variables in a Planck cosmology instead of the early time variables. This is only for the numerical considerations, and the accuracy compared from `camb` [[reference]]is found to be better than 1%. This approach is

[1] The Planck 2015 chains (Planck Collaboration et al. 2015) are not available when this work is undergoing

applied to each cosmological models described above and thus speeds the computation significantly.

The resulting compression of the CMB data is represented by a simple Gaussian distribution with mean of the data vector

$$\mu_{\mathbf{v}} = \begin{pmatrix} 0.02245 \\ 0.1393 \\ 94.27 \\ 0.03448 \end{pmatrix} \tag{70}$$

and its covariance

$$C_{\mathbf{v}} = \begin{pmatrix} 1.29\times10^{-7} & -6.04\times10^{-7} & 1.43\times10^{-5} & 3.45\times10^{-8} \\ -6.04\times10^{-7} & 7.55\times10^{-6} & -3.41\times10^{-5} & -2.36\times10^{-7} \\ 1.43\times10^{-5} & -3.41\times10^{-5} & 4.24\times10^{-3} & -6.60\times10^{-7} \\ 3.45\times10^{-8} & -2.36\times10^{-7} & -6.60\times10^{-7} & 2.20\times10^{-7} \end{pmatrix}. \tag{71}$$

For more details of the CMB compressed data, we refer the readers to Aubourg et al. (2015).

2.2.4. *Supernovae data*

Type-Ia supernovae (SNe) are considered as "standard candles" to probe the expansion history of the universe by measuring the luminosity distance as a function of redshift. In this paper, we use the Joint Light-curve Analysis (JLA) sample (Betoule et al. 2014) in the calculation, which is constructed from the SDSS-II Supernova Survey (Sako et al. 2014) and the Supernova Legacy Survey (SNLS) 3-year data set (Conley et al. 2011) combined with several samples of low redshift SNe. For simplicity, we here use the compressed representation of the relative distance constraints rather than the full `cosmomc` module. The compressed data is described by a vector in 31 redshift bins, as well as the covariance matrix. Note that absolute luminosity of SNe is considered uncertain and therefore, the fiducial absolute magnitude is marginalized out.

2.2.5. *Hubble constant H_0*

The Hubble constant (H_0) is an important quantity which provides clues about the visible expansion of the universe. The CMB measurements tell us a lot of physics during the early time, and provide constraints about some late time quantities. However, the CMB-inferred measurement of H_0 is model dependent, and the comparison with the one measured locally is a test of the standard cosmological model. In this paper, we employ the analysis of Riess et al. (2016) which yields a 2.4% determination of the quantity

$$H_0 = 73.24 \pm 1.74 \mathrm{kms}^{-1}\mathrm{Mpc}^{-1}. \tag{72}$$

This value is 3.4σ higher than the result from Planck data. This tension may imply new physics beyond standard model or GR. For instance, one plausible explanation could involve an additional source of dark radiation in the early Universe (Riess et al. 2016).

3. METHODOLOGY OF GOODNESS OF FIT

As mentioned earlier in the introduction, one of the aims in this paper is to evaluate the goodness of fit for each model introduced in Section 2.1 and therefore select the models that can explain the data with the highest confidence. The comparison of the model and the data is realized by the χ^2 statistics. Indeed, the χ^2 statistics are good at finding the best-fit parameters of a model, but insufficient to select the best model among various candidates (Davis et al. 2007). This statistical problem of model selection has been an active research field in modern cosmology and we have gained significant progress (Hobson et al. 2002; Saini et al. 2004; Mukherjee et al. 2006; Heavens et al. 2007).

One of the widely accepted method about model selection is by the use of the Bayes factor. For a given model M with parameter vector θ, the posterior probability given the data vector D is

$$p(M|D) = \frac{p(D|M)p(M)}{p(D)}. \tag{73}$$

The evidence is defined as

$$p(D|)\mathrm{M} = \int d\theta p(D|\theta, M)p(\theta|M) \tag{74}$$

For two models M and M' with non-committal priors that we want to compare, $p(M) = p(M')$, the ratio of their evidence leads to the Bayes factor

$$B \equiv \frac{\int d\theta' p(D|\theta', M')p(\theta'|M')}{\int d\theta p(D|\theta, M)p(\theta|M)} \tag{75}$$

This ratio evaluates which model is favored by the data. The realization of the Bayes factor involves the integration of the likelihood function over the parameter space. This procedure is usually computationally expansive especially when the model has a large parameter space. Furthermore, the Bayes factor can only be used for nested models, where the simpler model is a special subclass of the more generalized model. This restriction limits the use of Bayes factor in the investigation of dark energy and modified gravity models.

Another model selection strategy is the information criteria (Liddle 2004), specifically the Akaike information criterion (Akaike 1974, hereafter AIC) and the Bayesian information criterion (Schwarz et al. 1978, hereafter BIC). They are defined as

$$\begin{aligned} \mathrm{AIC} &= -2\ln\mathcal{L} + 2k, \\ \mathrm{BIC} &= -2\ln\mathcal{L} + k\ln N, \end{aligned} \tag{76}$$

where $\mathcal{L}$ is the maximum likelihood, k is the number of parameters of the model, and N is the number of data points used in the fit. The forms of AIC and BIC have different origins in information theory, but they determine the best model in the same manner that the model minimizes AIC or BIC is favored. Indeed, both the Bayes evidence and information criteria are consistent with the principle of Occam's razor: the simpler model is always favored as long as it provides nearly as good fit as the more complicated model. In Bayes evidence strategy, due to this principle, the more complicated model receives the penalty from the larger parameter volume. Similarly, in information criteria, the more complicated model gets the penalty from the second term as in Eq. (76). Just like Bayes evidence, the information criteria have limitations themselves. The penalty term just depends on the dimension of the data set and the number of model parameters. In other words, the models with different

physical motivations but the same number of parameters receive the same amount of punishment. This is not necessary to be true, because the models have different structures in their parameter space. For instance, the two-dimensional parameterizations of the equation of state Eq. (10, 11, 12) and the early dark energy model Eq. (19) have the same complexity from the information criteria point of view, but they fit the data from different aspects in the sense that the values of the parameters and their degeneracies are not the same. Therefore the penalty from complexity should be a model-dependent quantity in information criteria.

In this paper, we propose an alternative to investigate the model selection problem: the examination of the p-value. The p-value is defined as the probability of obtaining data that are a worse fit to the model, assuming that the model is correct (Davis et al. 2007). In a χ^2-based likelihood analysis, the p-value can be easily computed with the minimum of χ^2 and the degree of freedom for a given model and dataset. Therefore, the small value of p-value indicates that the model has a high probability to be an outlier and can be rejected (Strictly speaking: the data are unlikely to have happened if the Universe was really described by the model considered.) (Verde 2010). This method has been applied in some cosmological model selection researches, see Davis et al. (2007); Aubourg et al. (2015) and references therein. However, we should note that this calculation of p-value assumes that the errors in the measurements are Gaussian distributed and the model is linear in its parameters. These conditions are not satisfied for most of the models as described in Section 2.1, and the datasets are not strictly Gaussian distributed (the non-Gaussianity mainly come from the LyaF, BOSS CMASS and SDSS MGS BAO measurements). Therefore we should apply the method which is consistent with the essential concept of p-value. We describe this strategy as follows

1, For a given dataset and model, we find the maximum likelihood $\mathcal{L}$ with respect to the model parameter θ. The best-fit of the parameters $\hat{\theta}$ are the approximation of the true but unknown parameters Θ.

2, The value of $\mathcal{L}(\hat{\theta})$ reflects the goodness of fit between the model and the data. The p-value can be estimated from the distribution of $\mathcal{L}(\hat{\theta})$.

3, By the use of the variance from the real observations, we can generate an ensemble of random data sets from the true model (approximated by the best-fit model). The maximum likelihood $\mathcal{L}$ is searched for each of the realizations in the ensemble. The distribution of $\mathcal{L}$ worse than the one from the real dataset indicates the p-value, i.e. the probability that the real observation is an outlier assuming the model is true.

Fig. 2 shows the application of this method to the spatially flat ΛCDM model, which is the simplest model determined by only two parameters Ω_m and h for the geometrical probes. It is clear from the figure that the linear growth data $f\sigma_8$ are consistent with the other probes, because the increment of χ^2_{min} is smaller than the added number of data points. This is partly due to the relative large observational errors, and the narrow range of redshift distribution. On the other hand, the local Hubble constant H_0 shows significant tension with the other datasets. The addition of this single data point increases the χ^2_{min} by at least 5.5. This is consistent with the previous result from Planck and H_0 measurements (Planck Collaboration et al. 2014, 2015; Riess et al. 2016). The addition of H_0 also pushes the inferred p-value to the edge of about 2σ, but indeed the ΛCDM model is still a good fit to the data.

The result with the addition of spatial curvature Ω_k is displayed in Fig.3. The values of χ^2_{min} from each real datasets are smaller than Fig.2 which is consistent with expectation due to a small but non-zero curvature. The cumulative probability from the random ensemble is also left shifted because of the increased flexibility of the model. These two effects are canceled out to some extent and therefore the non-flat model doesn't show significant preference to the flat model (or even worse).

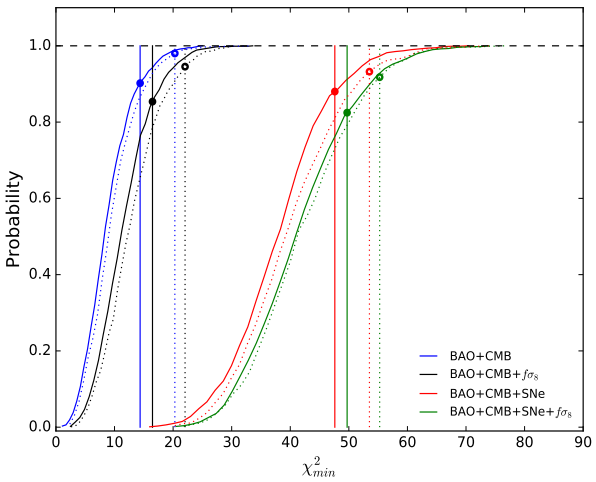

FIG. 2.— The p-value test of the flat ΛCDM model with different data combinations. The vertical lines correspond to the χ^2_{min} (or equivalently, the maximum likelihood $\mathcal{L}_{max}$) from the real observations. The non-verticle lines correspond to the cumulative probability from the distribution of $\mathcal{L}_{max}$ from the random ensemble, which has one thousand realizations in this figure. The intersection points represented by the dots correspond to $1-p$, which indicates the consistency between the data and model. The dotted lines and empty dots correspond to the datasets plus the local Hubble constant H_0.

We apply this method to the models introduced in Section 2.1 and compare the inferred p-value from each datasets. As an example, Figure 4 displays the results of several parameterizations of w (Section 2.1.1), early dark energy (Section 2.1.6) and Polynomial CDM (Section 2.1.8) models. All these models can recover ΛCDM model by fixing some of the parameters. It is clear that the added complexity doesn't show significant preference than the ΛCDM model, which is consistent with the essence of the principle of Occam's razor, but the difference is small and only up to 2%. The application of the information criteria gives similar conclusion, but the penalty term in AIC or BIC is usually large, which may give stronger conclusion than the p-value test. Note that the cumulative probability may not be smooth for some model+data combinations, this is due to the finiteness of the random ensemble.

The results of the p-value test for the other models are presented with the MCMC test in the next section.

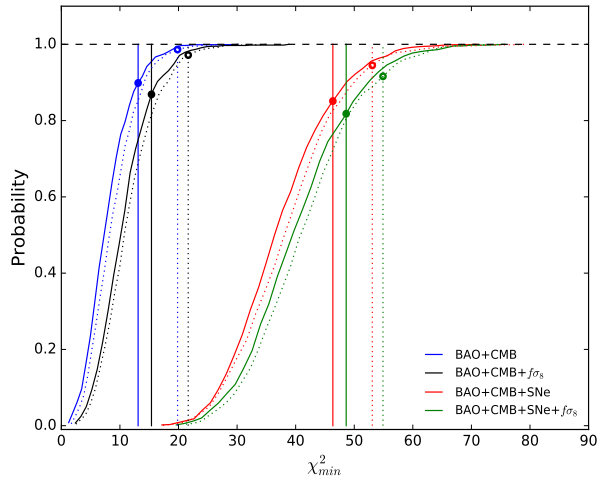

FIG. 3.— The same as Fig.2 but for ΛCDM with spatial curvature Ω_k.

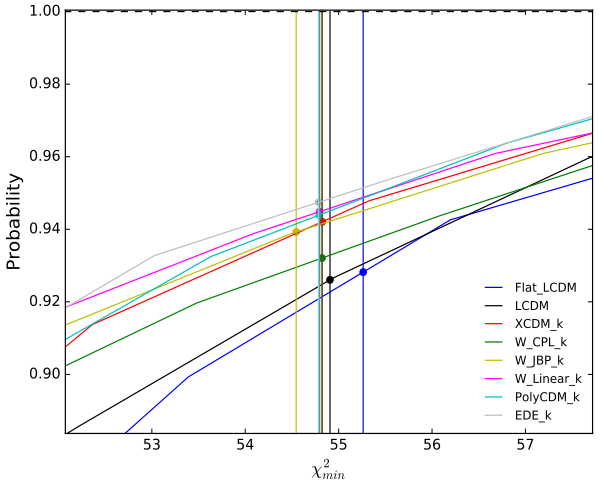

FIG. 4.— The p-value test for the models of several parameterizations of w and the early dark energy model by the use of all the datasets introduced in Section 2.2. For visualization purpose, the plot just shows the region around the intersection points. The "k" in the legend represents that the spatial curvature is a free parameter. The cumulative probability for some simpler model may be higher than more complex model in some χ^2_{min} region, this is the variance due to the finiteness of the random ensemble.

4. COSMOLOGICAL IMPLICATIONS FROM MCMC TEST

We now turn to the constraints on the cosmological models as described in Section 2.1 by the use of the python package `emcee` (Foreman-Mackey et al. 2013). The models that can recover the standard ΛCDM model always provide better (or at least equivalent) goodness of fit (smaller or identical χ^2_{min}). However, the p-value test of these models doesn't show statistical significant evidence to accept or reject them, therefore it is necessary to find the variance and constraint on their parameters. The results tell us the extent that the model deviates from standard ΛCDM model. Based on this, it is anticipated that the future experiments and observations will have the power to differentiate the models. On the other hand, some models don't have ΛCDM model as their special cases. The results of the p-value test on these models fall into two categories: clear evidence to reject, no clear evidence to reject or accept. For the former, the MCMC test tell us where the tensions between different datasets locate which in turn can support the result of p-value. For the later, it usually implies the possibility of physics beyond the standard model, and the MCMC test is necessary to examine the confidence level. We begin with the ΛCDM model and follow the sequence determined from the connections between the models.

Figure 5 shows the confidence regions and one-dimentional probability functions of the parameters for the non-flat ΛCDM model. The p-value test approves the consistency of the linear growth data with the geometrical probes. This two-dimensional figure shows the consistency among the geometrical probes, in particular between BAO and SNe. The impact of the H_0 data is evident from this figure, the best-fit value increases from X to X. The constraint on the spatial curvature Ω_k doesn't show strong deviation from flatness, $\Omega_k = 0$ is well within the 1σ region for all the data sets combined.

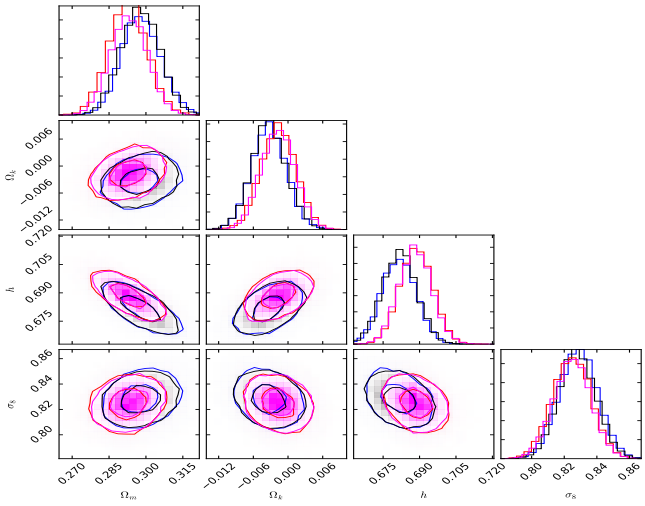

FIG. 5.— The 68.7% and 95.0% confidence regions of the parameters for non-flat ΛCDM. The diagonal panels show the one-dimensional probability distribution functions.

4.1. *Parameterization of equation of state w*

The simple parameterizations of the equation of state of dark energy w is a direct way to study its dynamical behavior, which is one of the important questions in the DE research. As an example, Figure 6 presents the constraints on the CPL parameterization. These classes of dark energy models have some results in common, firstly, the SNe data strongly favor a constant w, while the BAO data imply a non-zero w_1 but $w_1 = 0$ is in the 2σ region. Secondly, the distribution of h for different datasets varies significantly (need more), the addition of SNe data can lift the tension caused by H_0 observation at some extent.

The Pseudo-Nambu Goldstone Boson (PNGB) model has a well motivated physical background, but the cos-

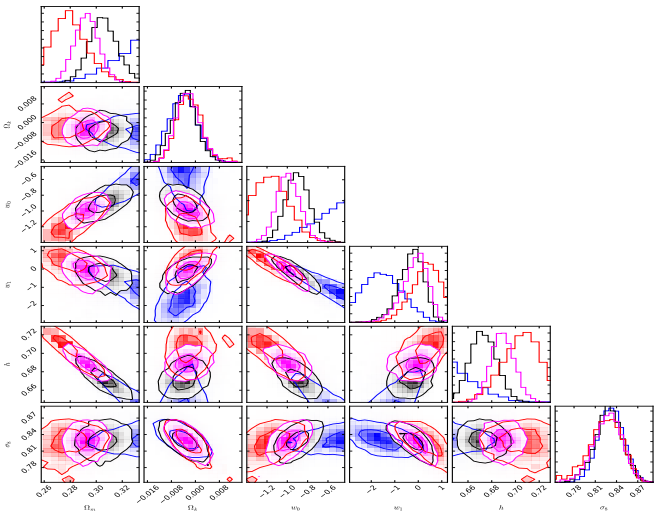

FIG. 6.— The 68.7% and 95.0% confidence regions of the parameters for non-flat CPL parameterization of w. The diagonal panels show the one-dimensional probability distribution functions.

mological solution is represented by a parameterization of w, which is a perturbation around -1. In this model, we find similar results as the CPL model. The constraint on the parameters are displayed in Figure 7. The parameter F is restricted into a limited range due to the numerical considerations, but it is clear to see that the upper bound is much larger than illustrated, which suppresses the deviation of w from -1, especially the constraint on w_0 is also near -1.

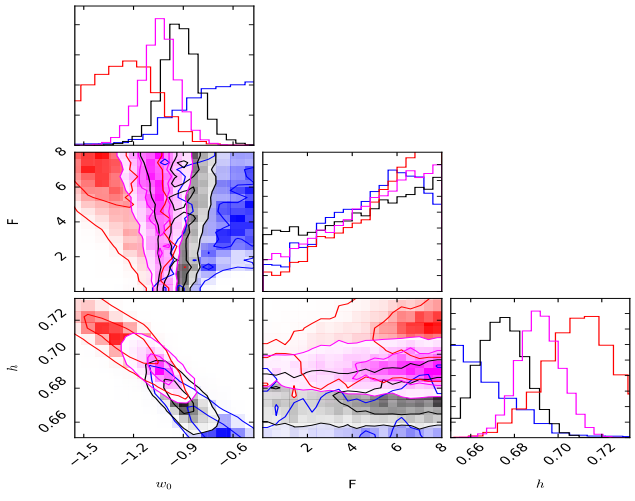

FIG. 7.— The 68.7% and 95.0% confidence regions of the parameters w_0, F and h for non-flat PNGB model. The diagonal panels show the one-dimensional probability distribution functions.

4.2. *Casimir effect*

4.3. *Cardassian expansion*

4.4. *Early dark energy*

Figure 8 presents constraints on the early dark energy model from the purely geometrical probes. The dark energy component has effects on early time and leave its

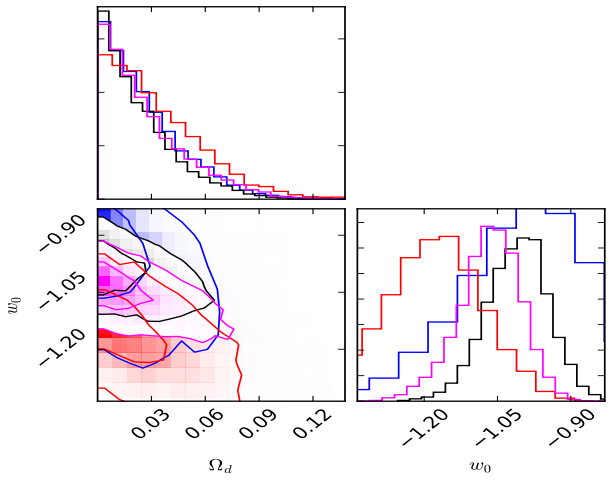

FIG. 8.— The 68.7% and 95.0% confidence regions of the parameters Ω^e_{de} and w_0 for non-flat early dark energy model. The diagonal panels show the one-dimensional probability distribution functions.

footprint on the matter perturbation. However, the data constraint suggests a negligible energy fraction, therefore the addition of the linear growth data doesn't show any apparent signal. The different data combinations give consistent results about Ω^e_{de}. The upper bound $\Omega^e_{de} < 0.07$ is in agreement with the previous investigations (Doran & Robbers 2006; Aubourg et al. 2015)

4.5. *Slow roll dark energy*

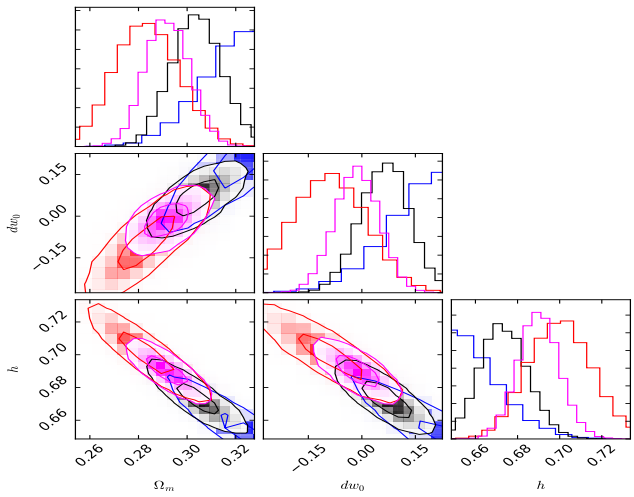

FIG. 9.— The 68.7% and 95.0% confidence regions of the parameters Ω^e_{de} and w_0 for non-flat early dark energy model. The diagonal panels show the one-dimensional probability distribution functions.

The slow roll dark energy scenario has the same number of parameters as the XCDM model. The constraints from a joint fit are shown in Figure 9, which yields $\delta w_0 = X$ ..... A small non-zero value of δw_0 is found with the datasets, but this departure is negligible considering the statistical significance.

4.6. *parameterization of Hubble parameter*

include PolyCDM, oscillation and logarithm hubble parameter.

4.7. *Chaplygin gas*

4.8. *Interacting DE and DM*

4.9. *Weakly-coupled canonical scalar field*

4.10. *Holographic dark energy*

4.11. *Quintessence scalar field model*

4.12. *QCD ghost dark energy and DGP cosmology*

4.13. *$f(R)$ gravity*

4.14. *$f(T)$ gravity*

4.15. *Galileon cosmology: Tracker solution*

4.16. *Kinetic gravity braiding model*

5. DISTRIBUTIONS OF OBSERVABLES

The previous results about the model selection and parameter constraints are based on the current data. The measurements of the distance scales from BAO and SNe, and the linear growth data from the galaxy survey can make predictions of the observables at various redshift ranges. These predictions from different cosmological models can be tested by the future experiments. Where the predictions are weak, the observables can be used to estimate parameters of the model, and where they are strong, the precision measurements can potentially falsify the dark energy or modified gravity models (Mortonson et al. 2009). Therefore in this section, we present the predictions of the observables for each model, and compare with the forecast from the future experiments, including the eBOSS (Dawson et al. 2016; Zhao et al. 2016) and DESI (Levi et al. 2013).

Figure 10 shows the predictions of the observables for the non-flat ΛCDM model, the parameters are selected from the MCMC test with all the datasets combined. The flat ΛCDM model is assumed to be a fiducial model and the quantities are displayed with respect to its predictions. This figure shows the effect of a non-zero Ω_k. Due to the simplicity of this model, the predictions are tight which means a significant non-zero Ω_k can be easily falsified by the future experiments. In particular, the forecast of the linear perturbation observations from DESI in redshift range $0.7 < z < 1.5$ is worth expectation since the model prediction has highest accuracy.

Figure 11 shows the prediction of the Oscillating Ansatz (OA, Section 2.1.9) as an example which is much more flexible than the ΛCDM model. The theoretical predictions reveal its oscillating nature which can fit a small data sample much better than the other models. However this better fit is not inherited by larger and evenly spaced data sample. Therefore the p-value test doesn't present much preference of this model. Note that the difference of the OA scenario and the ΛCDM model is clear from the figure, therefore as we accumulate more data pints in the future, the constraints on this model can be improved obviously and the falsification can be easily reached.

6. DISCUSSION AND CONCLUSION

REFERENCES

Akaike, H. 1974, IEEE transactions on automatic control, 19, 716
Amendola, L. 2000, Phys. Rev. D, 62, 043511
Amendola, L., Gannouji, R., Polarski, D., & Tsujikawa, S. 2007a, Phys. Rev. D, 75, 083504
Amendola, L., Polarski, D., & Tsujikawa, S. 2007b, Physical Review Letters, 98, 131302
Anderson, L., Aubourg, É., Bailey, S., et al. 2014, MNRAS, 441, 24
Arcos, H. I., & Pereira, J. G. 2004, International Journal of Modern Physics D, 13, 2193
Astier, P. 2001, Physics Letters B, 500, 8
Aubourg, É., Bailey, S., Bautista, J. E., et al. 2015, Phys. Rev. D, 92, 123516
Bamba, K., Geng, C.-Q., Lee, C.-C., & Luo, L.-W. 2011, Journal of Cosmology and Astroparticle Physics, 1, 021
Barreiro, T., Copeland, E. J., & Nunes, N. J. 2000, Phys. Rev. D, 61, 127301
Basilakos, S., Plionis, M., & Lima, J. A. S. 2010, Phys. Rev. D, 82, 083517
Bean, R., & Doré, O. 2004, Phys. Rev. D, 69, 083503
Bean, R., Flanagan, É. É., Laszlo, I., & Trodden, M. 2008, Phys. Rev. D, 78, 123514
Bekenstein, J. D. 1973, Phys. Rev. D, 7, 2333
—. 1981, Phys. Rev. D, 23, 287
Bekenstein, J. D. 1994, Phys. Rev. D, 49, 1912
Benaoum, H. B. 2002, ArXiv High Energy Physics - Theory e-prints, hep-th/0205140
Bengochea, G. R., & Ferraro, R. 2009, Phys. Rev. D, 79, 124019
Bento, M. C., Bertolami, O., & Sen, A. A. 2002, Phys. Rev. D, 66, 043507
Betoule, M., Kessler, R., Guy, J., et al. 2014, A&A, 568, A22
Beutler, F., Blake, C., Colless, M., et al. 2011, MNRAS, 416, 3017
Bilić, N., Tupper, G. B., & Viollier, R. D. 2002, Physics Letters B, 535, 17
Bordag, M., Mohideen, U., & Mostepanenko, V. M. 2001, Phys. Rep., 353, 1
Bordemann, M., & Hoppe, J. 1993, Physics Letters B, 317, 315
Cai, R.-G. 2007, Physics Letters B, 657, 228
Cai, R.-G., Tuo, Z.-L., Wu, Y.-B., & Zhao, Y.-Y. 2012, Phys. Rev. D, 86, 023511
Caldera-Cabral, G., Maartens, R., & Schaefer, B. M. 2009, Journal of Cosmology and Astroparticle Physics, 7, 027
Caldwell, R. R. 2002, Physics Letters B, 545, 23
Caldwell, R. R., Dave, R., & Steinhardt, P. J. 1998, Physical Review Letters, 80, 1582
Caldwell, R. R., & Kamionkowski, M. 2009, Annual Review of Nuclear and Particle Science, 59, 397
Caldwell, R. R., Kamionkowski, M., & Weinberg, N. N. 2003, Physical Review Letters, 91, 071301
Capozziello, S., Cardone, V. F., Carloni, S., & Troisi, A. 2003, International Journal of Modern Physics D, 12, 1969
Capozziello, S., & Fang, L. Z. 2002, International Journal of Modern Physics D, 11, 483
Capozziello, S., Farooq, O., Luongo, O., & Ratra, B. 2014, Phys. Rev. D, 90, 044016
Chevallier, M., & Polarski, D. 2001, International Journal of Modern Physics D, 10, 213
Chiba, T., Sugiyama, N., & Nakamura, T. 1997, MNRAS, 289, L5
Chimento, L. P., Jakubi, A. S., Pavón, D., & Zimdahl, W. 2003, Phys. Rev. D, 67, 083513
Cognola, G., Elizalde, E., Nojiri, S., Odintsov, S. D., & Zerbini, S. 2005, Journal of Cosmology and Astroparticle Physics, 2, 010
Cohen, A. G., Kaplan, D. B., & Nelson, A. E. 1999, Physical Review Letters, 82, 4971
Conley, A., Guy, J., Sullivan, M., et al. 2011, ApJS, 192, 1
Cooray, A. R., & Huterer, D. 1999, ApJ, 513, L95
Copeland, E. J., Liddle, A. R., & Wands, D. 1998, Phys. Rev. D, 57, 4686

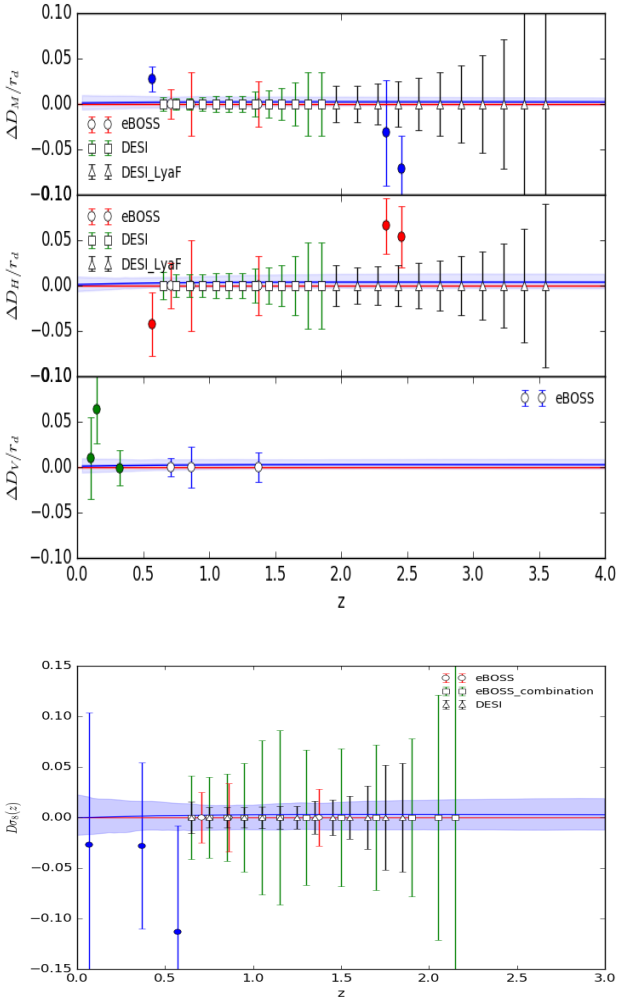

FIG. 10.— The predictions of the observables for non-flat ΛCDM model. *Top panel* : the BAO distance scales; *Botton panel* : $f\sigma_8$ from the linear perturbation theory. The horizontal red line is the prediction from flat ΛCDM model, the solid dots with errorbars represent current observations, the empty dots with errorbars are the forecast from future experiments, the blue line is the prediction from the non-flat ΛCDM model and the shaded region is the 1σ errors. All the quantities are displayed with respect to flat ΛCDM model.

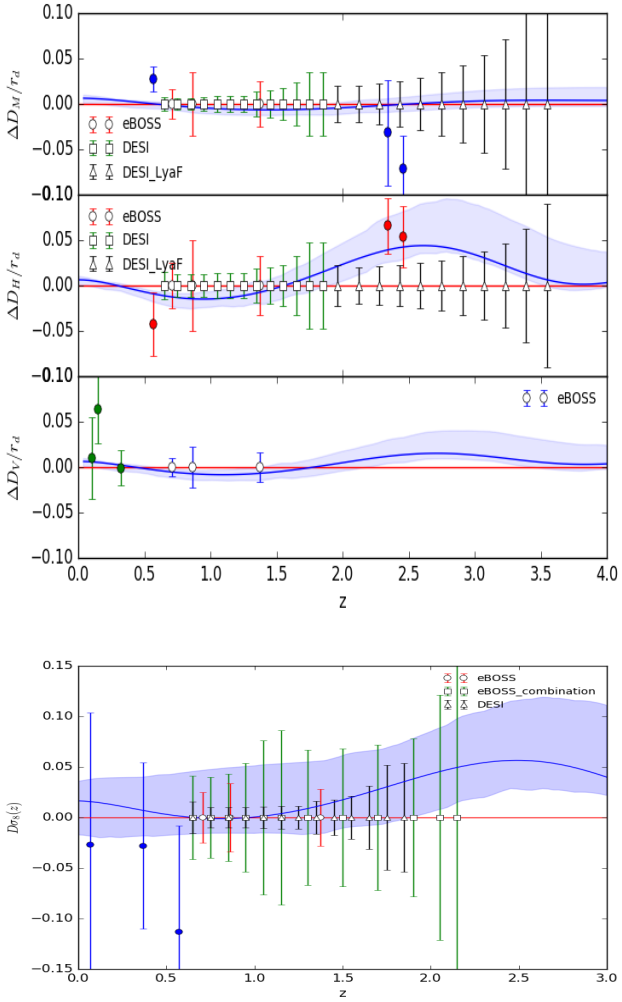

FIG. 11.— The same as Figure 10 but for OA scenario.

Copeland, E. J., Sami, M., & Tsujikawa, S. 2006, International Journal of Modern Physics D, 15, 1753
Dalal, N., Abazajian, K., Jenkins, E., & Manohar, A. V. 2001, Physical Review Letters, 87, 141302
Davis, T. M., Mörtsell, E., Sollerman, J., et al. 2007, ApJ, 666, 716
Dawson, K. S., Kneib, J.-P., Percival, W. J., et al. 2016, AJ, 151, 44
de Felice, A., Kase, R., & Tsujikawa, S. 2011, Phys. Rev. D, 83, 043515
Deffayet, C., Deser, S., & Esposito-Farèse, G. 2009a, Phys. Rev. D, 80, 064015
Deffayet, C., Esposito-Farèse, G., & Vikman, A. 2009b, Phys. Rev. D, 79, 084003
Deffayet, C., Pujolàs, O., Sawicki, I., & Vikman, A. 2010, Journal of Cosmology and Astroparticle Physics, 10, 026
Delubac, T., Bautista, J. E., Busca, N. G., et al. 2015, A&A, 574, A59
Dodelson, S., Kaplinghat, M., & Stewart, E. 2000, Physical Review Letters, 85, 5276
Doran, M., & Robbers, G. 2006, Journal of Cosmology and Astroparticle Physics, 6, 026
Dutta, K., & Sorbo, L. 2007, Phys. Rev. D, 75, 063514
Dvali, G., Gabadadze, G., & Porrati, M. 2000, Physics Letters B, 485, 208
Einstein, A. 1928, Riemann-Geometrie mit Aufrechterhaltung des Begriffes des Fernparallelismus (Wiley Online Library)
Eisenstein, D. J., Zehavi, I., Hogg, D. W., et al. 2005, ApJ, 633, 560
Faraoni, V., & Dolgov, A. 2002, International Journal of Modern Physics D, 11, 471
Farrar, G. R., & Peebles, P. J. E. 2004, ApJ, 604, 1
Fay, S. 2016, MNRAS, 460, 1863
Ferraro, R., & Fiorini, F. 2007, Phys. Rev. D, 75, 084031
—. 2008, Phys. Rev. D, 78, 124019
Font-Ribera, A., Kirkby, D., Busca, N., et al. 2014, Journal of Cosmology and Astroparticle Physics, 5, 027
Foreman-Mackey, D., Hogg, D. W., Lang, D., & Goodman, J. 2013, PASP, 125, 306
Freese, K., & Lewis, M. 2002, Physics Letters B, 540, 1
Frieman, J. A., Hill, C. T., Stebbins, A., & Waga, I. 1995, Physical Review Letters, 75, 2077
Gao, C., Wu, F., Chen, X., & Shen, Y.-G. 2009, Phys. Rev. D, 79, 043511
Giannantonio, T., & Melchiorri, A. 2006, Classical and Quantum Gravity, 23, 4125
Godłowski, W., & Szydłowski, M. 2006, Physics Letters B, 642, 13
Gott, J. R., & Slepian, Z. 2011, MNRAS, 416, 907

Hawking, S. W. 1976, Phys. Rev. D, 13, 191
Hayashi, K., & Shirafuji, T. 1979, Phys. Rev. D, 19, 3524
Heavens, A. F., Kitching, T. D., & Verde, L. 2007, MNRAS, 380, 1029
Hobson, M. P., Bridle, S. L., & Lahav, O. 2002, MNRAS, 335, 377
Hsu, S. D. H. 2004, Physics Letters B, 594, 13
Hu, W., & Sawicki, I. 2007, Phys. Rev. D, 76, 064004
Huang, Q.-G., & Li, M. 2004, Journal of Cosmology and Astroparticle Physics, 8, 013
Huang, Z., Bond, J. R., & Kofman, L. 2011, ApJ, 726, 64
Huterer, D., Kirkby, D., Bean, R., et al. 2015, Astroparticle Physics, 63, 23
Jassal, H. K., Bagla, J. S., & Padmanabhan, T. 2005, MNRAS, 356, L11
Joyce, A., Jain, B., Khoury, J., & Trodden, M. 2015, Phys. Rep., 568, 1
Kamenshchik, A., Moschella, U., & Pasquier, V. 2001, Physics Letters B, 511, 265
Karolyhazy, F. 1966, Il Nuovo Cimento A (1971-1996), 42, 390
Kawarabayashi, K., & Ohta, N. 1980, Nuclear Physics B, 175, 477
Kawarabayashi, K., & Ohta, N. 1981, Progress of Theoretical Physics, 66, 1789
Kimura, R., & Yamamoto, K. 2011, Journal of Cosmology and Astroparticle Physics, 4, 025
Levi, M., Bebek, C., Beers, T., et al. 2013, ArXiv e-prints, arXiv:1308.0847
Li, B., & Barrow, J. D. 2007, Phys. Rev. D, 75, 084010
Li, M. 2004, Physics Letters B, 603, 1
Liddle, A. R. 2004, MNRAS, 351, L49
Linder, E. V. 2003, Physical Review Letters, 90, 091301
—. 2008, Reports on Progress in Physics, 71, 056901
Linder, E. V. 2009, Phys. Rev. D, 80, 123528
—. 2010, Phys. Rev. D, 81, 127301
Lombriser, L., Hu, W., Fang, W., & Seljak, U. 2009, Phys. Rev. D, 80, 063536
Lombriser, L., Slosar, A., Seljak, U., & Hu, W. 2012, Phys. Rev. D, 85, 124038
Maluf, J. W. 1994, Journal of Mathematical Physics, 35
Maziashvili, M. 2007a, Physics Letters B, 652, 165
—. 2007b, International Journal of Modern Physics D, 16, 1531
Mortonson, M. J., Hu, W., & Huterer, D. 2009, Phys. Rev. D, 79, 023004
Mukherjee, P., Parkinson, D., & Liddle, A. R. 2006, ApJ, 638, L51
Nesseris, S., Basilakos, S., Saridakis, E. N., & Perivolaropoulos, L. 2013, Phys. Rev. D, 88, 103010
Nesseris, S., de Felice, A., & Tsujikawa, S. 2010, Phys. Rev. D, 82, 124054
Nesseris, S., & Perivolaropoulos, L. 2004, Phys. Rev. D, 70, 043531
Nicolis, A., Rattazzi, R., & Trincherini, E. 2009, Phys. Rev. D, 79, 064036
Nojiri, S., & Odintsov, S. D. 2003, Phys. Rev. D, 68, 123512
Ohta, N. 1981, Progress of Theoretical Physics, 66, 1408
—. 2011, Physics Letters B, 695, 41
Peebles, P. J., & Ratra, B. 2003, Reviews of Modern Physics, 75, 559
Peebles, P. J. E., & Ratra, B. 1988, ApJ, 325, L17
Perlmutter, S., Aldering, G., Goldhaber, G., et al. 1999, ApJ, 517, 565
Planck Collaboration, Ade, P. A. R., Aghanim, N., et al. 2014, A&A, 571, A16
—. 2015, ArXiv e-prints, arXiv:1502.01589
Randall, L., & Sundrum, R. 1999, Phys. Rev. Lett., 83, 4690
Randall, L., & Sundrum, R. 1999, Physical Review Letters, 83, 3370
Ratra, B., & Peebles, P. J. E. 1988, Phys. Rev. D, 37, 3406
Riess, A. G., Filippenko, A. V., Challis, P., et al. 1998, AJ, 116, 1009
Riess, A. G., Macri, L. M., Hoffmann, S. L., et al. 2016, ArXiv e-prints, arXiv:1604.01424
Rosenzweig, C., Schechter, J., & Trahern, C. G. 1980, Phys. Rev. D, 21, 3388
Ross, A. J., Samushia, L., Howlett, C., et al. 2015, MNRAS, 449, 835
Saini, T. D., Weller, J., & Bridle, S. L. 2004, MNRAS, 348, 603
Sako, M., Bassett, B., Becker, A. C., et al. 2014, ArXiv e-prints, arXiv:1401.3317
Sawicki, I., & Hu, W. 2007, Phys. Rev. D, 75, 127502
Schwarz, G., et al. 1978, The annals of statistics, 6, 461
Senovilla, J. M. M., Sopuerta, C. F., & Szekeres, P. 1998, General Relativity and Gravitation, 30, 389
Silvestri, A., & Trodden, M. 2009, Reports on Progress in Physics, 72, 096901
Slepian, Z., Gott, J. R., & Zinn, J. 2014, MNRAS, 438, 1948
Song, Y.-S., Hu, W., & Sawicki, I. 2007, Phys. Rev. D, 75, 044004
Sotiriou, T. P., & Faraoni, V. 2010, Rev. Mod. Phys., 82, 451
Starobinsky, A. A. 2007, Soviet Journal of Experimental and Theoretical Physics Letters, 86, 157
Susskind, L. 1995, Journal of Mathematical Physics, 36, 6377
't Hooft, G. 1993, ArXiv General Relativity and Quantum Cosmology e-prints, gr-qc/9310026
't Hooft, G. 2001, in Basics and Highlights in Fundamental Physics, ed. A. Zichichi, 72–100
Tocchini-Valentini, D., & Amendola, L. 2002, Phys. Rev. D, 65, 063508
Tsujikawa, S. 2007, Phys. Rev. D, 76, 023514
Turner, M. S., & White, M. 1997, Phys. Rev. D, 56, R4439
Unzicker, A., & Case, T. 2005, ArXiv Physics e-prints, physics/0503046
Urban, F. R., & Zhitnitsky, A. R. 2009a, Phys. Rev. D, 80, 063001
—. 2009b, Journal of Cosmology and Astroparticle Physics, 9, 018
—. 2010a, Physics Letters B, 688, 9
—. 2010b, Nuclear Physics B, 835, 135
Veneziano, G. 1979, Nuclear Physics B, 159, 213
Verde, L. 2010, in Lecture Notes in Physics, Berlin Springer Verlag, Vol. 800, Lecture Notes in Physics, Berlin Springer Verlag, ed. G. Wolschin, 147–177
Wang, Y., Freese, K., Gondolo, P., & Lewis, M. 2003, ApJ, 594, 25
Watson, C. R., & Scherrer, R. J. 2003, Phys. Rev. D, 68, 123524
Wei, H., & Cai, R.-G. 2008, Physics Letters B, 660, 113
Weinberg, D. H., Mortonson, M. J., Eisenstein, D. J., et al. 2013, Phys. Rep., 530, 87
Weinberg, S. 1989, Rev. Mod. Phys., 61, 1
Weller, J., & Albrecht, A. 2002, Phys. Rev. D, 65, 103512
Wetterich, C. 1988, Nuclear Physics B, 302, 668
Witten, E. 1979, Nuclear Physics B, 156, 269
Wu, P., & Yu, H. 2011, European Physical Journal C, 71, 1552
Zhang, X., & Wu, F.-Q. 2007, Phys. Rev. D, 76, 023502
Zhao, G.-B., Li, B., & Koyama, K. 2011, Phys. Rev. D, 83, 044007
Zhao, G.-B., Wang, Y., Ross, A. J., et al. 2016, MNRAS, 457, 2377
Zimdahl, W., Pavn, D., & Chimento, L. P. 2001, Physics Letters B, 521, 133